2013 American Control Conference (ACC)
Washington, DC, USA, June 17-19, 2013

Modeling and control of optical fiber micropositioning in a thermal adhesive

Eric N. Sihite, Zhen Qiu, and Kenn R. Oldham, *Member, IEEE*

***Abstract*— An actuation and control concept for alignment of optical fibers in compact imaging systems, namely endoscopic microscopy probes, is presented. The system uses a thermal adhesive to allow repeated positioning of the optical fiber, allowing partial compensation for alignment errors arising from mechanical settling and adhesive drying behavior during manual instrument assembly. A lumped-parameter dynamic model for temperature-dependent adhesive behavior is proposed, together with a simple integral controller. Experimental testing with a larger mock-up is used to verify that the dynamic model can replicate system behavior and to evaluate controller performance. Positioning of a 100 µm diameter fiber with 5 µm accuracy after 3-4 iterations is achieved in the prototype system.**

I. Introduction

Microelectromechanical Systems (MEMS) technology has provided a variety of miniaturized components for optical scanning applications, such as micro-mirrors, optical switches, adaptive mirror arrays, and active microlenses. While many chip-level integrated systems have been produced, in general it remains difficult to combine multiple micro-optical components with macro-scale components within very small integrated system footprints. Challenges include precise alignment of small components, dimensional changes due to environment or aging, and misalignment due to shocks or vibration.

One class of miniaturized optical systems for which assembly can be highly challenging is miniature microscopy systems for endoscopic use [1-3]. These systems typically require alignment of a fiber-coupled laser with multiple mirrors and/or lenses that perform scanning [4-5] and focusing in biological tissue [6]. For example, in dual-axes confocal microscopes, such as that in Fig. 1, two fibers must be precisely aligned to one another (either parallel or tilted at matching angles) [16,19]. To achieve precise alignment in small diameter (<5 mm) imaging probes, even with high-precision machining of fixtures and housings, fibers and other components must often be repeatedly adjusted and secured manually until alignment is adequate.

MEMS silicon optical bench (SiOB) technology is a proposed solution to precise optical alignment technology,

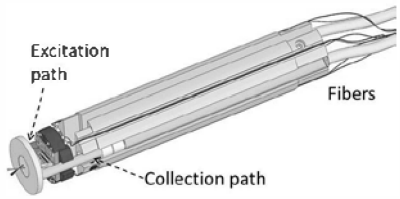

Figure 1. Dual-axes confocal microscope imaging head showing need for precise alignment of parallel image paths.

with passive fiber alignment mechanisms, such as v-grooves, often featuring alignment accuracies of ±1 to 2 microns [7-8], with passive fiber alignment mechanisms, such as v-grooves, often featuring alignment accuracies of ±1 to 2 microns [7-8], and some alignment mechanisms for smaller waveguides and micromirrors demonstrating sub-micron alignment [9-10]. However, when micromachined components must be further aligned with more traditionally-machined components, additional alignment errors may be seen. In the experience of the authors, 10 to 20 micron assembly accuracy is more representative in these situations, at least for endoscopic microscopy applications. In these cases, it may be desirable to provide active alignment capabilities for fibers or other micro-devices. A number of such alignment actuators exist [11-12] but these actuators are typically oriented around continually active applications, such as fiber switching or optical attenuation, rather than occasional alignment followed by fixed position operation.

This paper explores a potential method for automating alignment of optical fibers in small assembly areas using thermally-cycled adhesives and piezoelectric actuators. Actuators provide for small adjustments of fiber angle when the adhesive is melted while an appropriate control scheme moves the fiber into place, based on target positions that adapt over multiple iterations to adjust for shifts in fiber position when the adhesive solidifies. This approach is inspired by fiber positioning systems such as that by Unamuno et al. where UV curing after fiber positioning fixes optical components into place [13], demonstrated abilities to provide heating capabilities to SiOB assemblies [18], certain compact piezoelectric actuation schemes with substantial force and range of motion capabilities [14-15], and hands-on assembly experience in assembling dual-axes confocal microscopy systems of handheld (~10 mm diameter) dimensions.

Within the present work, a lumped-parameter dynamic model for the proposed system is described, and representative behavior of the system for positioning over the course of heating and cooling cycles is identified using a larger mock-up of such a system. A simple feedback control law and iteration scheme are proposed and tested in simulation and on the experimental setup.

*Research supported by National Institutes of Health.

E.N. Sihite was with the University of Michigan, Ann Arbor, MI 48109 USA. He is now with the University of California San Diego, San Diego, CA 92093 USA.

Z. Qiu is with the Department of Biomedical Engineering, University of Michigan, Ann Arbor, MI 48109 USA.

K.R. Oldham is with the Department of Mechanical Engineering and Applied Mechanics, University of Michigan, Ann Arbor, MI 48109 USA (e-mail: oldham@umich.edu; phone: 734-615-6327).

II. System Description and Parameter Estimation

A. System Description

The fiber positioning system consists of a glass fiber that extends from a fixed base past a piezoelectric unimorph actuator to a thermoelectric heating element that is coated with a thermally-controlled adhesive, as shown in Fig. 2. As the adhesive is heated, it softens and melts, allowing the actuator to adjust the fiber position. When the heater is turned off the adhesive cools and solidifies; during solidification, the actuator attempts to maintain fiber position, though some shifting is expected by the conclusion of cooling due to increasing surface forces, uneven cooling and thermal contraction. If this shift is repeatable, adjusting target fiber position during later heating cycles may achieve very precise fiber angles, without manual intervention.

For controller design, the fiber is described in lumped parameter form as a mass-spring-damper system subject to base excitation from the actuator (due to comparatively large actuator inertia) as well as stiffness and damping contributions from both the fiber (k_{fiber} and b_{fiber}, relatively constant) and adhesive (k_{adh} and b_{adh}, dependent on heater temperature, T), as represented in the form

$$m_{fiber}\ddot{x} + \left(b_{adh}(T) + b_{fiber}\right)\dot{x} + k_{adh}(T)\left(x - x_{0,adh}\right) + k_{fiber}x = b_{fiber}\dot{u} + k_{fiber}u \tag{1}$$

where m_{fiber} is effective fiber inertia, $x_{0,adh}$ is a potentially unknown nominal position determining stiffness behavior in the adhesive, and u is the input displacement imparted by an actuator. A block diagram of the system is shown in Fig. 3. If heating and cooling is iterated to improve fiber positioning, variables during the i-th iteration are denoted by superscript i, with $t^i = 0$ when heating commences. Two temperatures are identified as having particular significance during these cycles: T_{soft}, when localized melting begins, and T_{liq}, when the adhesive is observed to be entirely liquid. These temperatures are distinct due to uneven heating within the adhesive, though they are taken to be equivalent during cooling to the temperatures at which solidification begins and solidification is complete.

Effective adhesive stiffness is used as the primary method for modeling the solid to liquid transition. In other words, for modeling purposes $k_{adh}(T) \rightarrow k_{adh,0} >> k_{fiber}$ as T $\rightarrow$ 0 and $k_{adh}(T) \rightarrow 0$ when the adhesive is fully melted, with the specific function $k_{adh}(T)$ identified empirically (described for the prototype system in Section IV.B). given iteration i of a cooling and heating cycle, melting is denoted as being complete at time t_l^i and solidification is denoted as beginning at time t_{s0}^i, corresponding to the temperatures where the adhesive is first observed to be fully liquid or partially solid during experimental testing. Another way to state this is that for a single heating and cooling cycle i, the above times are defined such $T(t_l^i) = T_{soft}$ for increasing temperature, and $T(t_{s0}^i) = T_{liq}$ for decreasing temperature.

The settling or shifting of the adhesive as it cools is taken into account by representing the shift as the effective "stretch" in of the adhesive, $x - x_{0,adh}$, beginning when the adhesive starts to solidify at time t_{s0}^i. This stretch, in turn, is hypothesized as having a repeatable, position-dependent component correlated with fiber location when cooling occurs plus a random fluctuation, w. Mathematically, this defines $x_{0,adh}^i$ according to

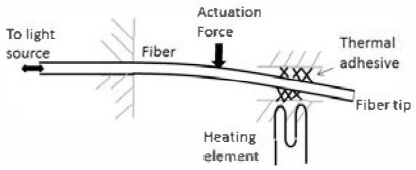

Figure 2. Concept drawing of fiber positioning system based on cycleable thermal adhesive.

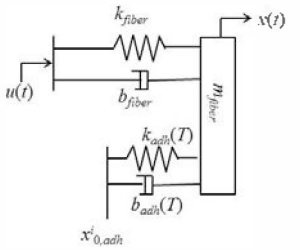

Figure 3. Lumped-parameter representation of positioning system

$$x^i(t_{s_0}^i) - x_{0,adh}^i = \Delta x_{adh}\left(x^i(t_{s_0}^i)\right) + w^i. \tag{2}$$

To summarize the adhesive behavior in the model over multiple cycles, the hypothesized force imparted on the fiber by the adhesive as a function of temperature becomes, $f_{adh}(T)$, becomes:

$$f_{adh}^i(T^i) = \begin{cases} -b_{fiber}(T^i)\dot{x} + k_{fiber}(T^i)\left(x_{0,adh}^{i-1} - x\right), & T < T_{liq}, \dot{T} > 0 \\ -b_{fiber}(T^i)\dot{x}, & T \geq T_{liq} \\ -b_{fiber}(T^i)\dot{x} + k_{fiber}(T^i)\left(x_{0,adh}^{i} - x\right), & T < T_{liq}, \dot{T} < 0 \end{cases} \tag{3}$$

with the above formulation assuming a single heating period and cooling period are performed in a given control cycle.

Inputs to the system are thermoelectric heater input voltage, V, and piezoelectric actuator input voltage, v, with each input having its own internal dynamics. A first-order linear model is used to represent the thermal dynamics,

$$\tau\dot{T} = -T + g_{heat}(V - V_t) \tag{4}$$

where τ is the heater time constant, g_{heat} is heater gain, and and V_t is a threshold voltage (relevant for the solid-state heating plate used in proof-of-concept experiments. A second-order, underdamped linear model is used to represent piezoelectric actuator dynamics,

$$m_{act}\ddot{u} + b_{act}\dot{u} + k_{act}u = g_{PZT}v \tag{5}$$

where m_{act}, b_{act}, and k_{act} are effective inertia, damping, and stiffness coefficients for the piezoelectric actuator, and g_{PZT} is the actuator gain. This model does not include hysteresis in the piezoelectric actuator as its influence on actuator motion in the prototype mock-up was found to be comparatively small (equivalent to less about 5% variation in effective actuator gain, g_{PZT}), although hysteresis could be included to further improve model accuracy. Both inputs are subject to saturation constraints, V_{max} and v_{max} according to:

$$0 \leq V \leq V_{\max}, \quad -v_{\max} \leq v \leq v_{\max} \tag{6}$$

III. Controller Design

The feedback controller for positioning the power has two components: a real-time feedback loop that drives the fiber to

a desired target position, r_i, during each iteration, and an adaptation law for r_i intended to eliminate the repeatable portion of the positional shift during cooling, Δx_{adh}.

The iterative portion of the controller is intended to drive fiber position to a specified final position, x_d, after cooling occurs, despite lack of prior knowledge of Δx_{adh}. An iterative control law of the form

$$r_i = r_{i-1} + a_1\left(x_d - \lim_{t\to\infty} x^{i-1}(t)\right) + \left(x_d - \lim_{t\to\infty} x^{i-2}(t)\right) \quad (7)$$

In this form, in the absence of the random portion of cooling shift, w, the target position is in equilibrium only when the cooled position of the fiber remains at x_d, i.e.

$$\lim_{t\to\infty} x^{i-1}(t) = r_i - \Delta x_{adh} = x_d \quad (8)$$

In this ideal response without random disturbance, constants a_1 and a_2 may be selected by the designer to define a desired transient response in adapted target positions. Naturally, in the real application, some random fluctuation is unavoidable.

The iterative controller in (7) assumes that while the adhesive is melted, the fiber can be effectively positioned at iterative target r_i by a real-time controller. This real-time controller is applied to the system in discrete time with sampling time Δt. Because the effective stiffness of the system is very large at low temperatures, two assumptions are made: first, that it is infeasible to select a sampling rate that is faster than Nyquist over the entire temperature range; second, that temperature varies slowly enough for thermal dynamics to be neglected during controller design.

The objectives of the real-time controller are then:

- Zero steady-state error at a constant temperature
- Stability at all temperatures anticipated during implementation
- Bounded amplitude of oscillations above the Nyquist frequency

These conditions are fulfilled through the use of an integral controller with a saturation limit,

$$v^i(t+\Delta t) = v^i(t) + K_I\left(r_i - .x^i(t)\right)$$
$$v_{\min C} < v^i(t+\Delta t) < v_{\max C} \quad (9)$$

where K_I is the integral gain and $v_{\min C}$ and $v_{\max C}$ are saturation limits that are typically, but not required to be, equal to the limits from (6). This control law is effective due to its steady-state error rejection properties and the fact that for the plant consisting of two underdamped systems in series, it is possible to select a K_I small enough to maintain a stable discrete-time response throughout a wide range of temperature dependent $k_{adh}(T)$ and $b_{adh}(T)$, so long as no discrete-time zero occurs on the real axis to the right of $z = 1$. A sample simulated response with an adhesive having linear dependence on temperature, taken from preliminary testing,

$$k_{adh} = 0.40 - 0.0061T$$
$$b_{adh} = 0.06 - 0.0001T \quad (10)$$

and with nominal cooling offset of 5 μm and random cooling offset variance also of 5 μm is shown in Fig. 4. This simulated response shows the desired behavior of the system, with the integral controller bringing the fiber to the target position in each iteration, and adaptation of the individual iteration targets intended to improve final position. In this simulation, the cooling shift is treated as an instantaneous event at the time that the adhesive temperature reaches the solidification temperature, and no sensor noise is included.

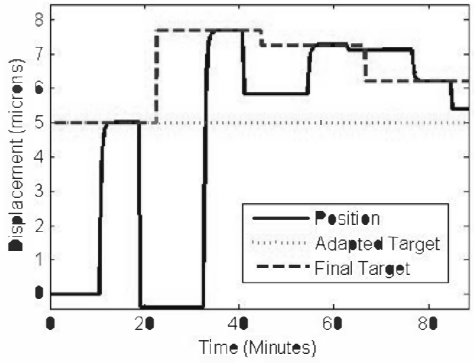

Figure 4. Simulated controller response for a linear adhesion model without sensor noise and with instantaneous cooling shift, showing adaptation of iteration targets and improvement in final fiber position.

IV. Experimental Testing

A. Experimental Setup

To test the modeling and control scheme, a meso-scale experiment was constructed at approximately ten times the length scales of a real endoscopic imaging probe. A glass 850nm wavelength optical fiber was supplied with light from a laser diode. The actuated portion of the fiber was stripped to its inner core, consisting of glass with a 100 μm diameter. 3.5 cm of stripped fiber were extended from a fixture for the flexible, position-controlled section. Actuation was performed 1.5 cm from the fiber base with a PhysikInstrumente GmbH lead-zirconate-titanate (PZT) bimorph actuator with center brass shim, 15 mm in length, 3 mm in width, and 0.4 mm in thickness. The final 0.5 cm of the fiber were projected over a thermoelectric Peltier heater, with approximately a 0.5 mm gap between fiber and heating surface. A sketch of the experimental setup is shown in Fig. 5. The thermal adhesive used was Crystalbond™ 555 adhesive, with listed softening temperature of 54° C [17].

Fiber position was measured using a photodiode attached to a linear amplifying circuit and recorded with an Arduino microcontroller interfaced to a PC. Photodiode and amplifer output was calibrated to produce a 1 bit change in ADC output for each 1 um on displacement. The Arduino microcontroller was also used to perform feedback control,

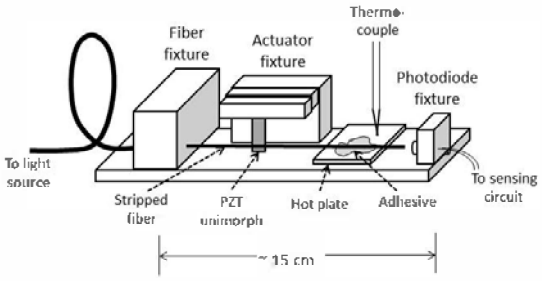

Figure 5. Experimental apparatus sketch.

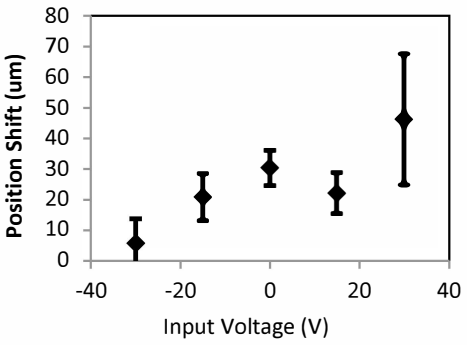

Figure 7. Total and ranges of shift in fiber position during adhesive solidification as function of applied open-loop voltage, showing repeatable portion of cooling shift larger than random fluctuations at most positions.

seen, the controller effectively moves the fiber to position with limited overshoot and minimal steady-state error as the adhesive melted. When the adhesive resolidified, relatively consistent shifts were observed, with average shift of -15 µm and standard deviation of 1.8 µm. This is consistent in magnitude with the identified shift obtained during the open-loop characterization previously shown in Fig. 4 and with less variance between cooling cycles. It is important to note that the controller attempts to maintain the fiber at its position during the period, and thus shifts appear to be a consequence of surface tension/solidification forces over-powering the piezoelectric actuator as the adhesive cools. While cooling cycles are much slower than heating cycles, fiber positioning is generally achieved with small overshoots and settling time dictated primarily by the thermal response. Fig. 9 shows the control input during the experiment with fixed position target, showing saturation of the actuator as the fluid cools and applies increasing unbalanced force to the actuator, as well as the variation in input voltage required to maintain the fiber at the origin from iteration to iteration

Fig. 10 shows closed-loop positioning results when the target position for each iteration is adapted in an attempt to counteract displacement forces. A final target position of 4 µm was selected, to test whether the iterative control could adjust fiber position to a resolution similar to the non-repeatable component position shifts. Starting reference was the origin. The control law for target adjustment was

$$r_i = r_{i-1} + 0.5 \cdot \left(x_d - \lim_{t\to\infty} x^{i-1}(t)\right) + 0.25 \cdot \left(x_d - \lim_{t\to\infty} x^{i-2}(t)\right) \quad (13)$$

which would produce a slightly underdamped response in ideal operation.

Best results for iterative adjustment were found in the 3rd heating and cooling cycle, with positioning error improved from approximately 8 µm to 5 µm after cooling. Additional iterations failed to substantially improve error from the eventual target. Notably, cooling shifts with target adaptation were much more irregular than with a constant target, possibly due to some form of hysteresis for controlled motions from positions alternating above and below the final target, or greater importance of PZT hysteresis than expected with alternating saturation values. Thus, under the current

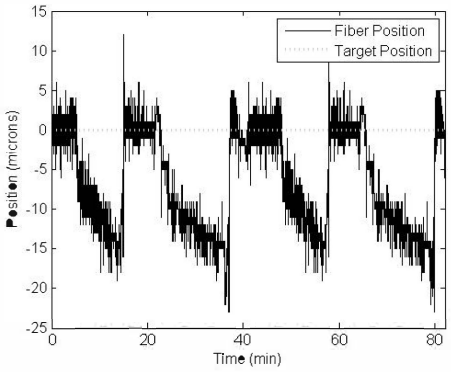

Figure 8. Fiber position versus time over four heating and cooling cycles (beginning with heated adhesive) for fixed target position at origin, showing consistent position shift during adhesive cooling and return to reference position upon heating.

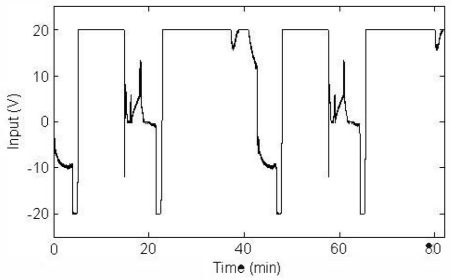

Figure 9. Control input during closed-loop testing with fixed target position, showing actuator saturation during cooled state and variation in input level when adhesive melted.

design, there remains a significant element of "luck" in improving final position in combination with the adaptive target algorithm. As a consequence, while target adaptation was able to modestly improve positioning error, the primary benefit of an active fiber positioning system appears likely to derive chiefly from the ability to do fine positioning in an automated way (improving positioning error from about 20 µm to 8 µm in experiments with the scaled mock-up).

Fig. 10 shows control effort during the experiment with adapted target positions, showing similar behavior to the control input during the fixed target tests, but with saturation limits alternating from low to high, possibly contributing to the less regular cooling shifts.

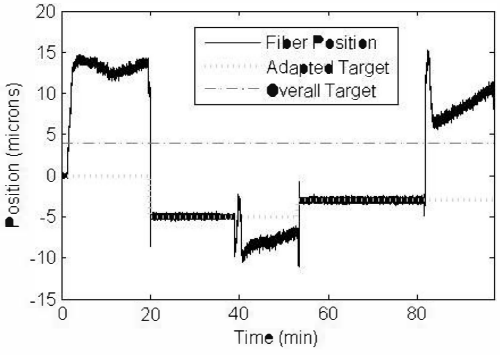

Figure 10. Fiber position versus time over three heating and cooling cycles (beginning with heated adhesive) for an adaptive target position with initial adapted target at origin and final target position of +5 µm.

V. CONCLUSIONS

An approach to adjustable and iterative positioning of an optical component (glass optical fiber) in complex optical systems was proposed and tested using a scaled-up experimental testbed. The approach relies on repeated heating and cooling of a thermal adhesive, coupled with iterative positioning of the optical fiber using real-time control. An empirical model of the thermal adhesive suitable for controller design was developed, and used to guide design of a simple integral controller with iteratively-adapted positioning target. In the scaled prototype, fiber position accuracies of approximately 5 µm were achieved. Accuracy is limited by adhesive solidification behavior at the final stage of cooling, such that refined iterative procedures that result in less perturbation of the melted adhesive in each iteration may be desirable.

Whether the proposed actuation and control concept can improve alignment in optical imaging instruments, such as a dual-axes confocal microscope, depends on a number of factors, as the existing mock-up is comparatively simple relative to target applications. While the current positioning accuracy is worse than previously demonstrated fiber alignment by passive silicon optical bench techniques to an SiOB itself, the controlled approach can adapt for other sources of misalignment between micromachined and conventionally machined structures, which is typically much larger. Also of critical importance will be the scaling of the disturbance forces during cooling for smaller structures and higher melting temperatures. In future work, these phenomena will be examined using bulk-micromachined test structures and fiber positioning controller tests. Future work will also examine the causes of larger cooling shift variance under iterative control than fixed target control only.

REFERENCES

[1] Y. Pan, H. Xie, and G.K. Fedder, G.K., "Endoscopic optical coherence tomography based on microelectromechanical mirror," *Optics Letters* vol. 26, no. 24, 2001, pp. 1966-1968.

[2] L. Fu, A. Jain, H. Xie, C. Cranfield, C., and M. Gu, "Nonlinear optical endoscopy based ona double-clad photonic crystal fiber and a MEMS mirror," *Optics Express*, vol. 14, no. 3, 2006, pp. 1027-1032.

[3] C. Chong, K. Isamoto, and H. Toshiyoshi, "Optically modulated MEMS scanning endoscope," *IEEE Photonics Tech. Letters,* vol. 18, No. 1, 2006, pp. 133-135.

[4] W. Piyawattanametha, L. Fan, S. Hsu, M. Fujino, M.C. Wu, P.R. Herz, A.D. Aguirre, Y. Chen, and J.G. Fujimoto, "Two-dimensional endoscopic MEMS scanner for high-resolution optical coherence tomography," *Conf. Lasers Electro-Optics*, San Francisco, CA, 2004.

[5] J. Singh, J.H.S. Teo, C.S. Premachandran, N. Chen, R. Kotlanka, M. Olivo, and C.J.R. Sheppard, C.J.R., "A two axes scanning SOI MEMS micromirror for endoscopic bioimaging," *J. Micromech. Microeng.*, vol. 18, no. 2, 2008, 025001.

[6] Z. Qiu, J.S. Pulskamp, C.-H. Rhee, T. Wang, R.G. Polcawich, and K. Oldham, "Large displacement vertical translational actuator based on piezoelectric thin-films." *J. Micromech. Microeng.*, vol. 20, no. 7, 2010, pp. 75016.

[7] M. Iwase, T. Nomura, A. Izawa, H. Mori, S. Tamura, T. Shirai, and T. Kamiya, "Single Mode Fiber MT-RJ SFF Transceiver Module using optical subassembly with a new shielded silicon optical bench," *IEEE Trans. Advanced Packaging,* vol. 24, no. 4, 2001, pp. 419-428.

[8] H.L. Hsiao, H.C. Lan, C.C. Chang, C.Y. Lee, S.P. Chen, C.H. Hsu, S.F. Chang, Y.S. Lin, F.M. Kuo, J.W. Shi and M.L. Wu, "Compact and passive alignment of 4-channel x 2.5 Gbps optical interconnect modules based on silicon optical benches with 45° micro-reflectors," *Optics Express*, vol. 17, no. 26, 2009, 24250.

[9] J. van Gurp, M. Tichem, M., and U. Staufer, "Design, fabrication and testing of assembly features enabling sub-micron accurate passive alignment of photonic chips on a silicon optical bench," *Adv. Info. Comm. Tech.*, vol. 371, 2012, pp. 17-27.

[10] O. Solgaard, M. Daneman, N.C. Tien, A. Friedberger, R.S. Muller and K.Y. Lau, "Optical packaging using silicon surface-micromachined alignment mirrors," *IEEE Photonics Tech. Letters*, vol. 7, no. 1, 1995, pp. 41-43.

[11] S.S. Lee, E. Motamedi, E. and M.C. Wu, "Surface-micromachined free-space fiber optic switches with integrated microactuators for optical fiber communication systems," *Conf. Solid State Sensors Actuators*, vol. 1, 1997, pp. 85-88.

[12] R. Jebens, W. Trimmer, W., and J. Walker, "Microactuators for aligning optical fibers," *Sensors and Actuators*, vol. 20, 1989, pp. 65-73.

[13] A. Unamuno, J. Yao, and D. Uttamchandani, "Alignment and fixing of fiber optics based on electrothermal MEMS actuators," *IEEE Photonics Tech. Letters*, vol. 17, no. 4, 2005, pp. 816-818.

[14] J. Domke, C.H. Rhee, Z. Liu, T.D. Wang, and K.R. Oldham, "Amplifying transmission and compact suspension for a low-profile, large displacement piezoelectric actuator," *J. Micromech. Microeng.*, vol. 21, 2011, 067004.

[15] K.Oldham, J.S. Pulskamp, R.G. Polcawich, and M. Dubey, "Thin-film PZT lateral actuators with extended stroke," *J. Microelectromech. Syst.*, vol. 17, no.4, 2018, pp.890-899.

[16] W. Piyawattanametha, H. Ra, Z. Qiu, S. Friedland, J.T.C. Liu, K. Loewke, G.S. Kino, O. Solvgaard, T.D. Wang, M.J. Mandella, C.H. Contag, "In vivo near-infrared dual-axis confocal microendoscopy in the human lower gastrointestinal tract," *J. Biomed. Opt.* vol. 17, no. 2, 2012, 021102.

[17] Structure Probe, Inc., "Crystalbond and wafer-mount mounting adhesives,"www.2spi.com, 2001.

[18] Y. Xu, M.F. Wang, C.S. Premachandran, K.W.S. Chen, N. Chen, and M. Olivo, "Platinum microheater integrated silicon optical bench assembly for endoscopic optical coherence tomography," *J. Micromechanics and Microengineering*, vol. 20, 2010, 015008.

[19] Z. Qiu, Z. Liu, X. Duan, S. Khondee, B. Joshi, M.J. Mandella, K. Oldham, K. Kurabayashi, T.D. Wang, "Targeted vertical cross-sectional imaging with handheld near-infrared dual axes confocal fluorescence endomicroscope," *Biomed. Opt. Expr.*, vol. 4, no. 2, 2013, pp. 3223-330.